Article

Enhanced Electrochemical and Safety Performance of Electrocatalytic Synthesis of NH₃ with Walnut Shell-Derived Carbon by Introducing Sulfur

Jin Wang [1], Zhichao Zheng [1], Bin Liu [1], Ziwei Wang [2,*] and Shuang Wang [3,*]

[1] College of Materials Science and Engineering, Advanced Energy Materials and Systems Institute, North University of China, Taiyuan 030051, China; 20210089@nuc.edu.cn (J.W.); s202203027@st.nuc.edu.cn (Z.Z.); liubin3y@nuc.edu.cn (B.L.)

[2] College of Mechanical Engineering, North University of China, Taiyuan 030051, China

[3] College of Environmental Science and Engineering, Taiyuan University of Technology, Jinzhong 030600, China

[*] Correspondence: 20140083@nuc.edu.cn (Z.W.); wangshuang@tyut.edu.cn (S.W.)

Abstract: An efficient catalyst is key to achieving the synthesis of electrochemical ammonia and improving safety. In this work, using biomass walnut shell as a carbon source and sodium thiosulfate as a sulfur source, sulfur-modified walnut shell-derived carbon material was synthesized via a simple low-temperature impregnation method at room temperature and atmospheric pressure as an effective electrochemical ammonia synthesis catalyst with high thermal stability. Scanning electron microscopy (SEM), transmission electron microscopy (TEM), Raman spectroscopy, X-ray photoelectron spectroscopy (XPS), nitrogen adsorption–desorption apparatus, thermogravimetry (TG), and other characterization methods were applied to analyze the micro-morphology and physicochemical structure of the electrocatalyst. The synthesized ammonia performance of the catalyst was measured using an ultraviolet (UV) spectrophotometer and electrochemical workstation. The catalyst design used the doping of sulfur atoms to create rich catalytic active sites, while the presence of elemental sulfur on the catalyst surface provided hydrophobicity, which was conducive to inhibiting competitive hydrogen evolution reaction (HER) and enhancing the electrocatalytic ammonia synthesis performance of the catalyst. Under normal temperature and pressure conditions, when a voltage of −0.45 V was applied, the ammonia yield in 0.05 M H₂SO₄ electrolyte was 10.39 μg$_{NH3}$ mg$_{cat.}^{-1}$ h^{-1}. The results showed that the introduction of sulfur effectively improved the electrocatalytic and thermal safety performance of bio-derived carbon materials, and the test presented that the performance of the catalyst was stable and reusable.

Keywords: electrocatalysis; non-metallic catalyst; sulfur modification; biomass porous carbon; thermal safety

1. Introduction

In this article, we reported on the development of a sulfur-modified walnut shell porous carbon catalyst (S/WSPC) for the electrochemical synthesis of ammonia under mild conditions. The traditional Haber–Bosch ammonia synthesis process is an energy-intensive production process with high energy consumption, large environmental pollution, and heavy dependence on non-renewable resources [1–5]. With the increasingly prominent environmental and resource problems, environmentally friendly alternative ammonia synthesis methods are gradually receiving close attention from scientists [6]. Due to the mild production conditions and green energy source, electrocatalytic ammonia synthesis is considered to be one of the best potential ammonia synthesis methods that can effectively reduce the energy crisis [7].

Since the N≡N bond of the N₂ molecule has three pairs of shared electrons, the dissociation energy is as high as 945.95 kJ·mol^{-1}, and it is hard to activate and be chemically inert.

Therefore, the catalytic conversion of the N_2 molecule needs to overcome a huge energy barrier, and an efficient electrocatalyst is urgently needed to activate the nitrogen molecule [8,9]. Compared with metal-based catalysts with high cost and scarce resources, carbon catalysts have the advantages of many sources, low cost, and controllable structure and have potential application prospects in the field of electrocatalysis [10]. Carbon materials are considered to be one of the most promising candidates because of their good electrical conductivity, surface modifiability, and acid and alkali corrosion resistance [11–14]. Among them, porous carbon has a large specific surface area, high pore volume, and adjustable pore structure and has been widely studied in catalysis, adsorption, energy storage, and other fields [12,15,16]. Based on the perspective of natural environmental protection and green economy, it is a wise decision to choose carbon materials derived from sustainable biomass. Generally, walnuts are a kind of nutrient-rich and beloved nuts, and the market demand is large, but the generated walnut shell waste is usually directly burned or dumped into a landfill, which aggravates environmental pollution [17]. The main components of the walnut shell are cellulose and wood, and the surface of cellulose contains hydroxyl functional groups, which makes it easy to achieve functional modification. However, the carbon material derived from biomass is inert in the electrocatalytic reaction, so developing the activity of carbon materials and enhancing the electrocatalytic performance are the research focus [18]. In recent years, the introduction of similar electronegative heteroatoms into carbon materials has been widely regarded as one of the most effective ways to improve the catalytic performance of carbon materials [19,20]. Since the doping of heteroatoms induces changes in the charge distribution of nearby carbon atoms, it can effectively regulate the electron-donating properties and surface polarity of adjacent carbon atoms, thereby changing the electronic state to provide a richer reactive site, especially in the activation of small molecules, showing better electrocatalytic performance [21–24]. For example, Pengfei Song et al. used sulfur-doped graphene to effectively improve the electrocatalytic degradation performance of organic dye methyl orange in graphene materials, proving that sulfur doping significantly enhanced the catalytic activity of carbon materials [25]. At present, sulfur doping methods are mainly achieved via the high-temperature pyrolysis of sulfur-rich precursors under the protection of inert gases (N_2 or Ar), but this process is complex and has high-energy consumption and a low yield [25–28].

The development of efficient and affordable electrocatalysts is essential for the practical realization of ammonia electrosynthesis. Our work provided a fresh and promising approach to the development of such catalysts. In this paper, a porous carbon material derived from walnut shell was introduced as a carrier, and sulfur was introduced into walnut shell carbon via a simple low-temperature impregnation synthesis method. Meanwhile, sulfur composite carbon derived from a walnut shell (S/WSPC) was obtained as an electrocatalyst for the electrochemical synthesis of ammonia under mild conditions. The analysis of the catalyst characterization results demonstrated that the S/WSPC catalyst had a rich cross-linked pore structure, which provided a rich space for N_2 adsorption, and the highly conductive biomass-derived carbon material provided an efficient electron transport channel for the electrocatalytic reaction, thereby improving the electrochemical reaction efficiency [15]. The introduction of sulfur provided a certain hydrophobicity on the catalyst surface, which helped to inhibit the water-resolved hydrogen competition reaction. The doped sulfur atom changed the electronic structure of the adjacent carbon atom and increased the defective structure of the walnut shell carbon material, thus creating rich synthetic ammonia active sites [29,30]. Under the optimum activation potential of -0.45 V (vs. RHE), the ammonia yield was 10.39 μg_{NH3} $mg_{cat.}^{-1}$ h^{-1} and the Faraday efficiency was 4.72%. This work provided a simple and efficient preparation method of sulfur modification and sulfur doping, proved the feasibility of the application of biomass-derived porous carbon in the electrochemical synthesis of ammonia, and enriched the research idea of electrocatalysts.
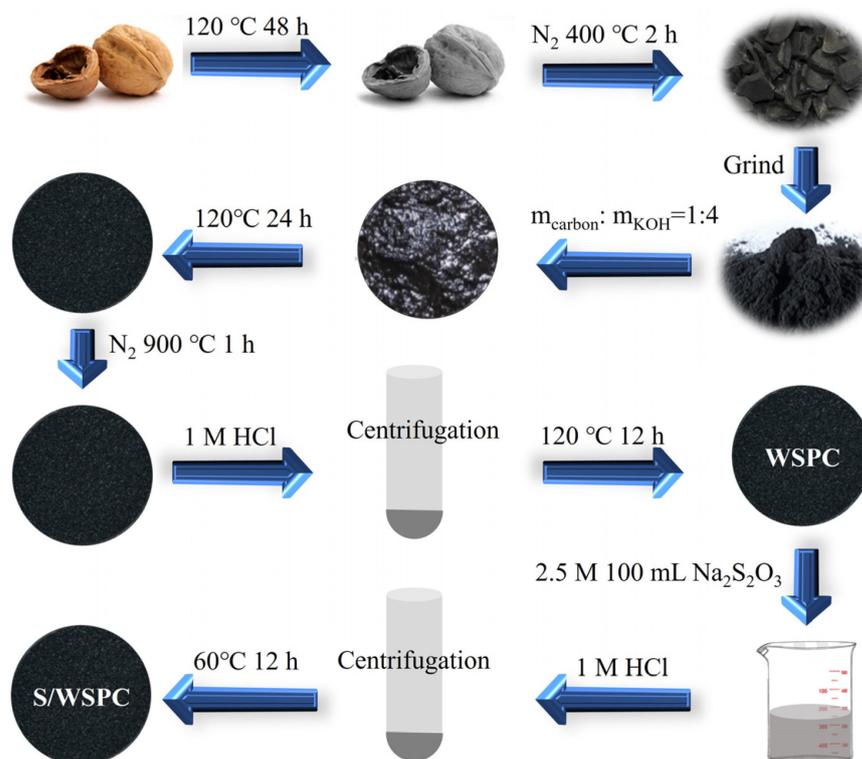
2. Experimental Materials and Methods

2.1. Materials

KOH, $Na_2S_2O_3$, N_2H_4, $Na_3C_6H_5O_7 \cdot 2H_2O$, $C_7H_6O_3$, $Na_2[Fe(CN)_5NO] \cdot 2H_2O$, NaClO, CH_4O_3S, NH_4Cl, CS_2 was purchased from Aladdin Industries, Nashville, TN, USA. Nafion (5%), carbon paper (C, 99%) purchased from Beijing Yinokai Technology Co., Ltd. (Beijing, China). HCl and ethanol were purchased from Sinopod Group Chemical Reagent Co., Ltd. (Shanghai, China). Nitrogen (N_2, 99.99%) and argon (Ar, 99.99%) were purchased from Taiyuan Anxu Hongyun Technology Development Co., Ltd. (Taiyuan, China).

2.2. Preparation of Porous Carbon in Walnut Shell

Walnut shell pretreatment: After the walnut shell was collected, it was dried and mashed. Soak them in deionized water and ethanol, respectively, and put them in a 120 °C oven for 48 h. After removal, it was put into a tube furnace for dry distillation. Under the protection of nitrogen gas, it was heated to 400 °C at a heating rate of 5 °C/min, kept warm for 2 h, and then lowered to room temperature at the same cooling rate. The charred walnut shell was removed. The charred walnut shell was pulverized and ground in a mortar for 30 min to obtain black carbon powder.

Walnut shell porous carbon (WSPC) preparation: According to the carbon-base mass ratio of 1:4, the corresponding quality of walnut shell carbon powder and KOH were weighed, mixed, and ground for 30 min, then put into a nickel crucible, drop an appropriate amount of deionized water, stir evenly to form a slurry mixture, and dry in a 120 °C oven for 24 h. The dried mixture is evenly placed in a quartz porcelain boat and placed in a tube furnace. In a nitrogen-protective atmosphere, the temperature was raised to 900 °C at a heating rate of 5 °C/min for 1 h and then lowered to room temperature at the same cooling rate. The activated toner was removed, and the unreacted KOH was neutralized with 1.0 M HCl after grinding for 30 min. The supernatant was neutral and then centrifuged with deionized water. The centrifugal toner was dried overnight in an oven at 120 °C to obtain black carbon powder WSPC. The electrocatalyst preparation process is shown in Scheme 1.

Scheme 1. The preparation flowchart of S/WSPC.

2.3. Preparation of Sulfur-Modified Walnut Shell Porous Carbon Catalyst

Preparation of S-doped walnut shell porous carbon (S/WSPC): 2.5 M aqueous solution of $Na_2S_2O_3$ was prepared, and an appropriate amount of WSPC powder was weighed and put into the solution. It was placed on the heated magnetic stirrer, with the temperature set to 60 °C, and stirred at a constant speed for 3 h so that the $Na_2S_2O_3$ solution was fully immersed in the pores of WSPC. Then, it was placed in the refrigerator to cool the mixed solution. After 30 min, it was removed. In the ice water bath, the pipette was used to slowly and uniformly add the pre-cooled HCl solution with a concentration of 1.0 M until the solution appeared milky and stopped. The mixture was refrigerated for 1 h to allow HCl to fully react with $S_2O_3{}^{2-}$ in WSPC holes. It was then removed to room temperature and centrifuged three times with deionized water. The centrifuged products were dried overnight in an oven at 60 °C and were recorded as S/WSPC. The preparation flowchart of S/WSPC is drawn in Scheme 1.

2.4. Electrocatalytic Performance Test

A conventional H-type electrolytic cell with a volume of 150 mL was used, where the counter electrode and reference electrode were composed of a Pt plate and silver/silver chloride electrode (Ag/AgCl, 1 M KCl solution), respectively. Platinum plate electrode clamp was selected as the working electrode in the experiment. Then, 0.05 M of H_2SO_4 was used as the electrolyte, and 70 mL of the electrolyte was added to the H-type cell in the experiment. The potential of the reference electrode and the standard hydrogen electrode was calculated using the following formula:

$$E_{RHE} = E_{(Ag/AgCl)} + 0.197 + 0.0591 \text{ pH} \tag{1}$$

Electrochemical testing techniques include linear sweep voltammetry (LSV) and chronoamperometry (CA). LSV was recorded at a scan rate of 10 mV/s between the applied potential of -1.5 and 0.0 V (vs. Ag/AgCl). In this experiment, LSV curves under Ar and N_2 saturation conditions were compared to determine whether the catalyst had nitrogen activation activity. Electrochemical conversions of N_2 to NH_3 for evaluation of Faradic efficiency and NH_3 formation rate were subsequently conducted using CA at a scan rate of 10 mV/s and applied potential of -0.45 V for 2 h.

2.5. Calculation Method of Ammonia Yield and Faraday Efficiency

(1)   Detection of $NH_4{}^+$ and N_2H_4

The concentrations of $NH_4{}^+$ and N_2H_4 should be calculated according to the standard concentration curve of $NH_4{}^+$ and N_2H_4. A standard solution with a concentration gradient of 0.1–1.0 μg/mL was prepared with ammonium chloride and N_2H_4. The linear equation of concentration–absorbance was drawn according to the absorbed light intensity values at 655 nm and 455 nm of the curve obtained via the UV absorbance test, respectively, and the concentrations of $NH_4{}^+$ and N_2H_4 in the sample liquid were calculated.

(2)   Faraday efficiency

Faraday efficiency was an important index to measure the utilization of electrons in electrochemical reactions. The calculation formula was

$$\text{Faraday Efficiency (FE)} = m\,NH_4{}^+ \times n \times F/17Q \tag{2}$$

where m was the mass of ammonia in the solution, n was the number of charges transferred during the reaction, F was the Faraday constant, the value 96,485.17 was the total number of protons in NH_3, and Q was the total number of charges during the timing current test.

2.6. Material Characterization

The surface morphology and structure of the experimental samples were characterized via scanning electron microscopy (SU8010, Hitachi, Japan) and transmission electron

microscopy (JEOL JEM-2100F, Hitachi, Japan). The degree of defect of carbon materials was analyzed via Raman spectrometer (inVia Reflex, Renishaw, UK) and powder X-ray diffractometer (Mini Flex II, Rigaku, Japan). The pore structure of the sample was characterized using a rapid physical adsorption assay (TriStar 2020, Micromeritics Instrument Corporation, Micromeritics, USA). Before the test, the sample was degassed at a vacuum of 100 °C for 5 h. Brunauer–Emmett–Teller (BET) method was used to calculate the specific surface area, and Barrett–Joyner–Halenda (BJH) was used to calculate the pore size distribution. X-ray photoelectron spectroscopy (Thermo Fisher Scientific K-Alpha XPS, Waltham, MA, USA) was used to analyze the valence states of elements. The ultraviolet visible spectrophotometer (Lambda 650, PerkinElmer, USA) tests the absorbance of the electrolyte. NH_4^+ had a test wavelength range of 500 to 800 nm, and N_2H_4 had a test wavelength range of 400 to 500 nm. The thermogravimetric analyzer (STA 449 F5, Netzsch, Germany) was used to test the thermal stability of the catalyst. Contact angle tester hydrophilicity of the sample, the CHNS element analyzer of varioELcube, performs precise analysis of the content of C, N, and S elements in the sample.

3. Experimental Results and Discussion

3.1. Material Characterization

3.1.1. SEM and EDS Characterization

The surface morphology of the samples was characterized via scanning electron microscopy (SEM). By calcination at high temperatures, the carbon particles of walnut showed irregular shape and uneven size. After sulfur modification, the morphology of S/WSPC was consistent with that of WSPC, but the morphology of particles was basically unchanged, which proved that the preparation method of low-temperature impregnation was mild and unspoiled the original morphology of the catalyst. In addition, there were some binding substances between S/WSPC particles, which may be a small amount of sulfur. The hydrophobicity of sulfur can enhance the hydrophobicity of the surface of the catalyst material, thus inhibiting the hydrogen evolution competitive reaction by preventing contact between the catalyst and water in the electrolyte. The SEM image in Figure 1c of the S/WSPC and corresponding EDS element mapping images show that the uniform distribution of C and S elements in S/WSPC can fully prove that the synthesis method uniformly modified sulfur on the surface of carbon materials, as shown in Figure 1d,e.
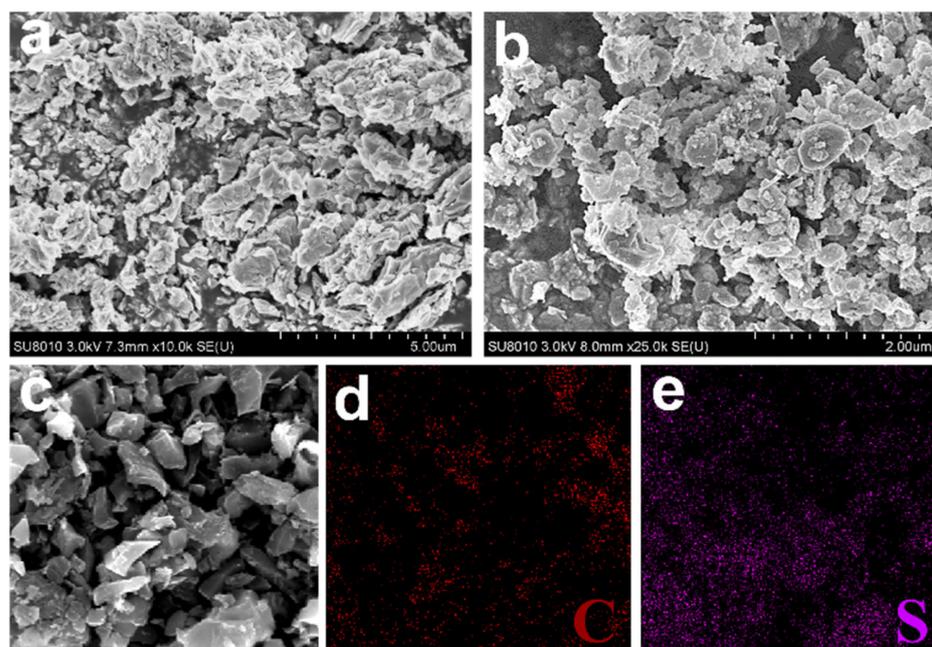

Figure 1. SEM images of (**a**) WSPC and (**b**) S/WSPC; (**c**) SEM diagram of S/WSPC and corresponding distribution diagram of (**d**) C, (**e**) S elements.

3.1.2. TEM

Figure 2a shows the TEM images of WSPC and S/WSPC. It can be seen that the two-dimensional sheet structure of graphene-like folds was obvious in the picture, indicating that the high-temperature carbonization process causes a high degree of graphitization of biomass carbon materials, which was conducive to electron transport in the electrochemical reaction process, and helps to improve the reaction rate and electron utilization rate [31]. As seen in Figure 2b, there are obvious black circular spot shadows distributed on the graphene-like two-dimensional flakes, which proved that the low-temperature synthesis process was mild to the sample morphology and will not damage the sample morphology. Combined with the published work, it was speculated that the circular spot shadows here may be sulfur spots, and other characterization results need to be analyzed and proved.
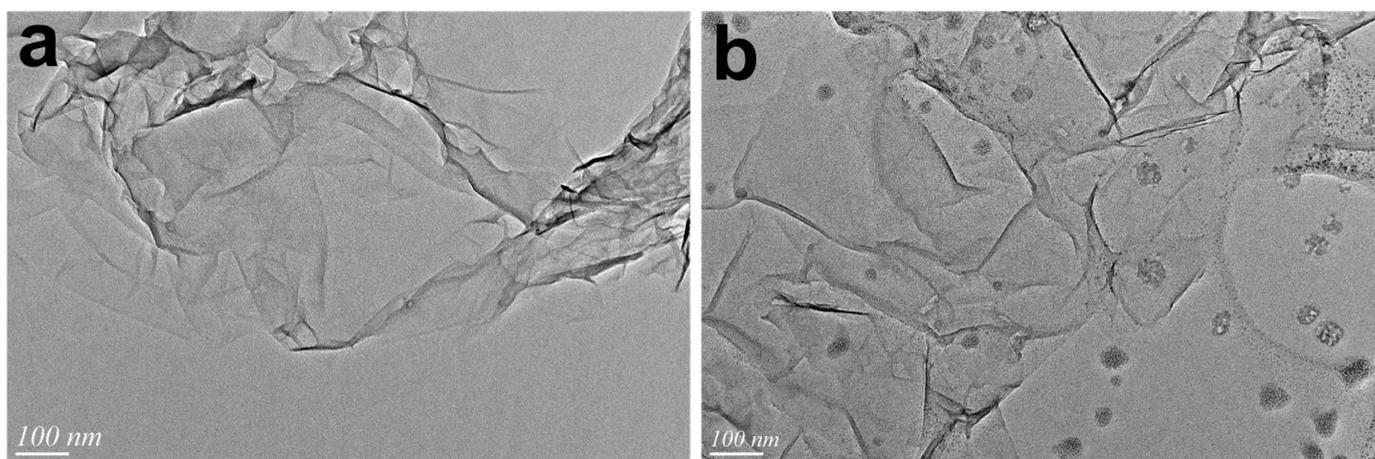

Figure 2. TEM images of (**a**) WSPC and (**b**) S/WSPC.

3.1.3. XRD and Raman

The crystal structure and defect degree of WSPS and S/WSPC were determined via powder X-ray diffraction (XRD) and Raman spectroscopy. The XRD patterns of WSPC and S/WSPC are shown in Figure 3a. In comparison, the shape of the curve after sulfur modification was unchanged, and the characteristic peak of the (002) crystal face of carbon material was wider at 2θ of 23°, which proved that sulfur modification did not change the graphitized crystal structure of WSPC. Notably, the diffraction peak signature of sulfur was not detected, which may be due to the tiny size of sulfur spots growing on the surface of the S/WSPC sample that were not detected. The tendency of the XRD characteristic peak of S/WSPC to shift to a small angle indicates that the increase in the lattice spacing of S/WSPC was presumed to be caused by the expansion of the layer spacing because the doped sulfur atom radius was obviously larger than that of the carbon atom, which becomes evidence supporting the successful doping of sulfur atom. In addition, the defect degree of S/WSPC was demonstrated in the test results of the Raman spectrometer, as shown in Figure 3b. The degree of disorder of carbon materials was usually expressed by the ratio of the intensity of D-peak (1358 cm^{-1}), which represents the disordered vibration caused by lattice vibration in carbon materials, to the intensity of G-peak (1595 cm^{-1}), which represented the disordered vibration caused by the in-plane vibration of carbon atoms. The test results showed that after the introduction of sulfur, the strength ratio of the two increased from 0.89 (WSPC) to 0.93 (S/WSPC), indicating that the disorder degree of the sulfur-modified catalyst increased. Combined with the analysis results of XPS, it can be seen that the doping of sulfur atoms led to a change in the electronic structure of adjacent carbon atoms, resulting in lattice distortion, which increased the defect and disorder degree of carbon materials [32]. This study displayed that the defects caused by doping are the active sites, so the increase in disorder represents the increase in catalytic active sites, which was conducive to the enhancement of catalytic activity.
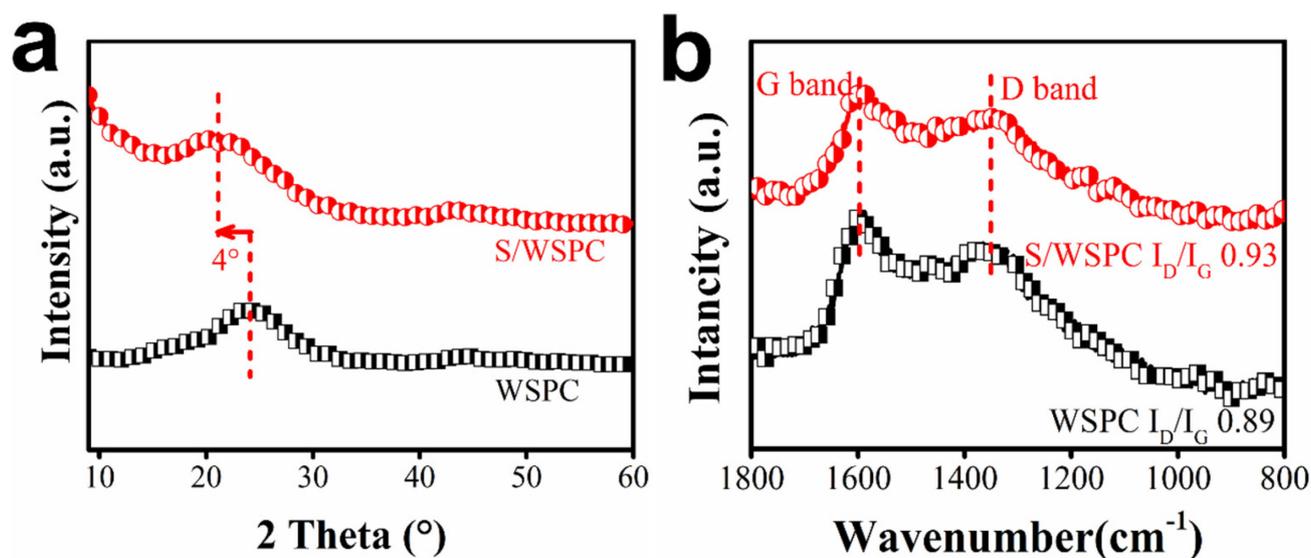
Figure 3. (**a**) XRD and (**b**) Raman of WSPC and S/WSPC.

3.1.4. XPS analysis

X-ray photoelectron spectroscopy (XPS) was used to characterize the surface element components and valence states of WSPC and S/WSPC. The corresponding test results are shown in Figure 4. The total XPS spectra of WSPC and S/WSPC showed the elements present in the catalyst. Compared with the C and N elements contained in WSPC (Figure 4a), S/WSPC Figure 4c) also detected an obvious characteristic peak of the S element, which fully proved the existence of the S element. The trace N elements in the two samples were derived from the nitrogen-containing functional groups in the biomass precursor. The C 1s spectrum of WSPC (Figure 4b) exhibited three characteristic peaks at the binding energy of 284.6, 285.4, and 289.4 eV, representing the three forms of carbon, namely C-C/C=C, C-O, and O-C=O, respectively. The C 1s and S 2p spectra of S/WSPC were shown in Figure 4d and 4e, respectively. The C 1s spectrum of S/WSPC had three characteristic peaks of 284.7, 285.4, and 289.3 eV, corresponding to the three forms of carbon, namely C-C/C=C, C-S/C-N, and O-C=O, respectively, indicating the existence of C-S bond in the sample, which proves the successful doping of S atom. The results were in agreement with the results of the XRD and Raman tests. The S 2p spectra of the S/WSPC samples showed three characteristic peaks in the binding energy of 164.0, 165.2, and 168.8 eV, belonging to C-S-C, C-S, and C-SO$_x$ bonds, respectively, which also indicated that the introduced sulfur element existed in a bonding mode with carbon atoms, demonstrating that S atoms were successfully doped into the carbon material of WSPC. The doping of the S atom affects the charge density of the adjacent C atom, and the resulting lattice distortion and lattice defect have strong adsorption and conversion ability to N$_2$, thus improving the electrocatalytic ammonia synthesis performance of the catalyst.
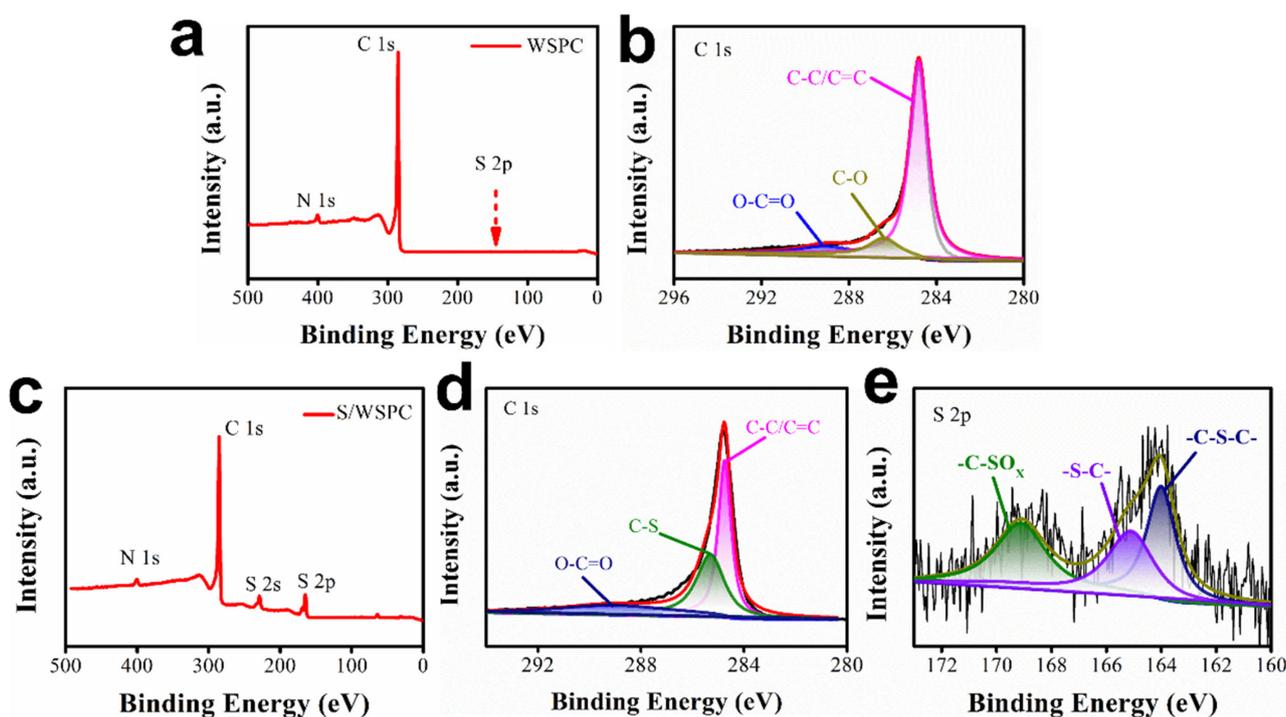
Figure 4. XPS spectra of WSPC (**a**) survey and (**b**) C 1s. XPS spectra of S/WSPC (**c**) survey, (**d**) C 1s and (**e**) S 2p regions.

3.1.5. Thermogravimetric (TG) Characterization, CHN Element Analysis and Contact Angle Test

The TG test results of WSPC and S/WSPC are shown in Figure 5a,b. Based on the low pyrolysis temperature of pristine sulfur, the content of pristine sulfur in carbon materials was quantitatively analyzed via thermogravimetric characterization. The DTG curve of WSPC was gentle, indicating that the weight loss process was tiny and sluggish. The mass loss of 6.3% during the process was caused by the deficiency of water in the sample and trace impurities in the carbon material. Compared with the DTG curve of WSPC, it could be seen that S/WSPC had three stages with significantly faster mass change rates, which are about 200 °C, 283 °C, and 440 °C, respectively, which correspond to the loss of bound water in the material, the process of melting and cracking of pristine sulfur via heat and evaporation and sublimation. This also proves the presence of pristine sulfur. According to the TG test results of S/WSPC, the content of pristine sulfur in S/WSPC was about 36.4%. Table 1 shows the contents of various elements in WSPC and S/WSPC measured using the CHN element analyzer. A small amount of N element comes from organic compounds contained in biomass carbon, among which the content of sulfur was 43.11%, which was close to the TG test result. Combined with the results of TEM and XPS, it can be seen that some sulfur atoms form carbon-sulfur bonds with the carbon atoms in contact at the same time as the formation of sulfur points, so sulfur atoms with bonds also exist in the material. Sulfur has excellent hydrophobicity, which can provide an effective hydrophobic protective film for the catalyst, effectively reduce the contact between the catalyst and water in the aqueous electrolyte, and thus inhibit the occurrence of HER competitive reaction. Figure 6 displays the contact angle test results of the hydrophobic carbon paper, WSPC, and S/WSPC, respectively. The results show that hydrophobic carbon paper has a high contact angle of 125.8°. After WSPC drops are applied to the surface of hydrophobic carbon paper, the hydrophobic value further increases, reaching 134.6°. It has reached the super hydrophobic level, which strongly proves that the hydrophobicity of the material after sulfur modification was significantly enhanced.
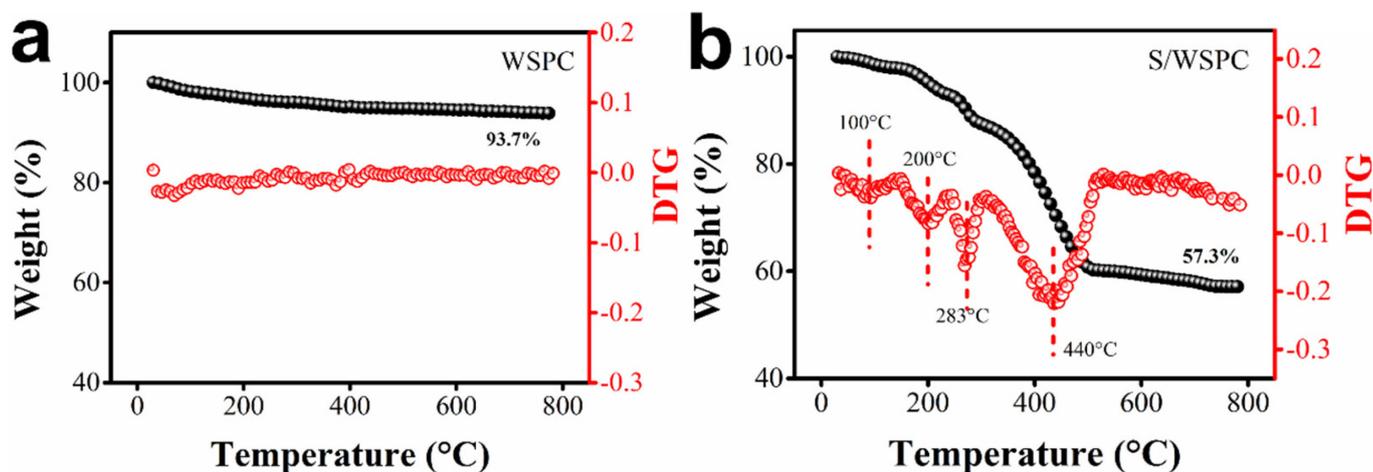
Figure 5. TG and DTG curves of (**a**) WSPC and (**b**) S/WSPC.

Table 1. The C, H, N, and S element content of WSPC and S/WSPC.

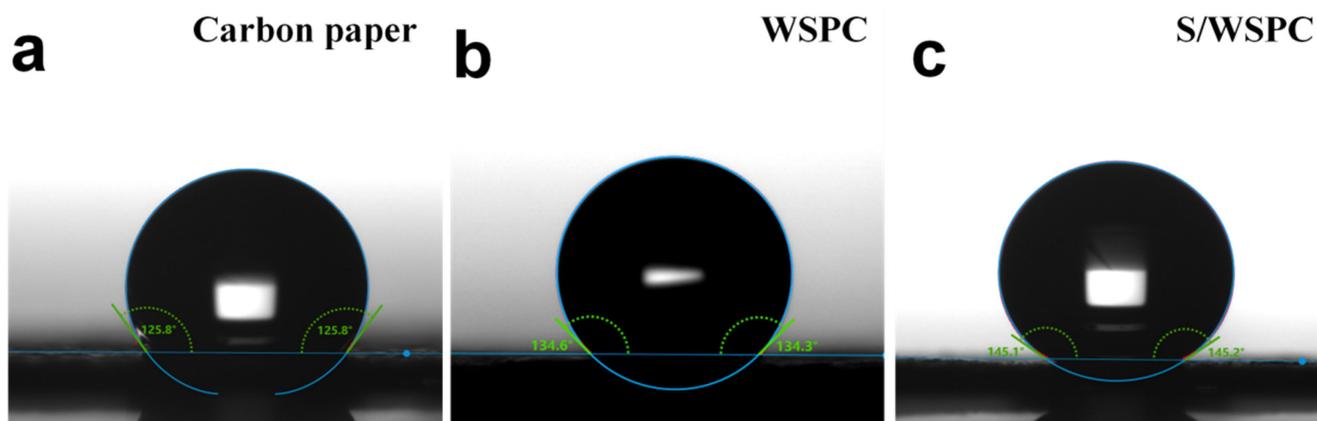| Element (wt%)	C	H	N	S
WSPC	91.125	0.589	2.562	0.000
S/WSPC	48.814	0.412	2.284	43.112

Figure 6. Contact angle test of (**a**) carbon paper, (**b**) WSPC, and (**c**) S/WSPC.

3.1.6. Nitrogen Isothermal Adsorption–Desorption Characterization

The pore structure of biomass carbon material was also one of the key factors affecting the adsorption and conversion performance of the catalyst. In order to understand the pore structure and pore size distribution of the catalyst, the N_2 adsorption–desorption isotherm was tested. Compared with the test results in Figure 7a,c, it can be seen that the N_2 adsorption–desorption curves of both are type I isotherms, indicating that both are microporous materials. Micropores are the main source of specific surface area in the pore material, which can greatly improve the specific surface area of the pore material, and a large number of micropores can be used as a barrier between the active substance and the electrolyte to prevent the dissolution of the active substance in the reaction, which was conducive to maintaining the structural stability of the electrocatalyst during the electrochemical reaction [33]. The presence of hysteresis loop in the N_2 adsorption–desorption isotherm of S/WSPC indicates that mesopore was introduced into S/WSPC, which proved that S/WSPC had the characteristics of layered pore structure, and mesopore structure was conducive to the infiltration of electrolyte and promote the electrochemical reaction. In the low-pressure region, the N_2 absorption rate of the desorption isotherm of S/WSPC

increased sharply compared with that of WSPC, indicating that the adsorption capacity of N_2 was strong, which was conducive to the enrichment of nitrogen near the catalytic active site. After testing, the BET-specific surface area of WSPC was 1993.50 m^2 g^{-1} and the pore volume was 1.03 cm^3 g^{-1}, while the BET-specific surface area of S/WSPC dropped to 362.97 m^2 g^{-1}, and the pore volume was 0.08 cm^3 g^{-1}, which was speculated to be due to the partial blocking of sulfur in the pores of carbon materials. The specific surface area of the material was reduced. Comparing the pore size distribution of WSPC and S/WSPC, it can be seen that the pore size distribution of S/WSPC was wide with a small number of mesopores, which may be caused by the reaccumulation of catalyst particles.
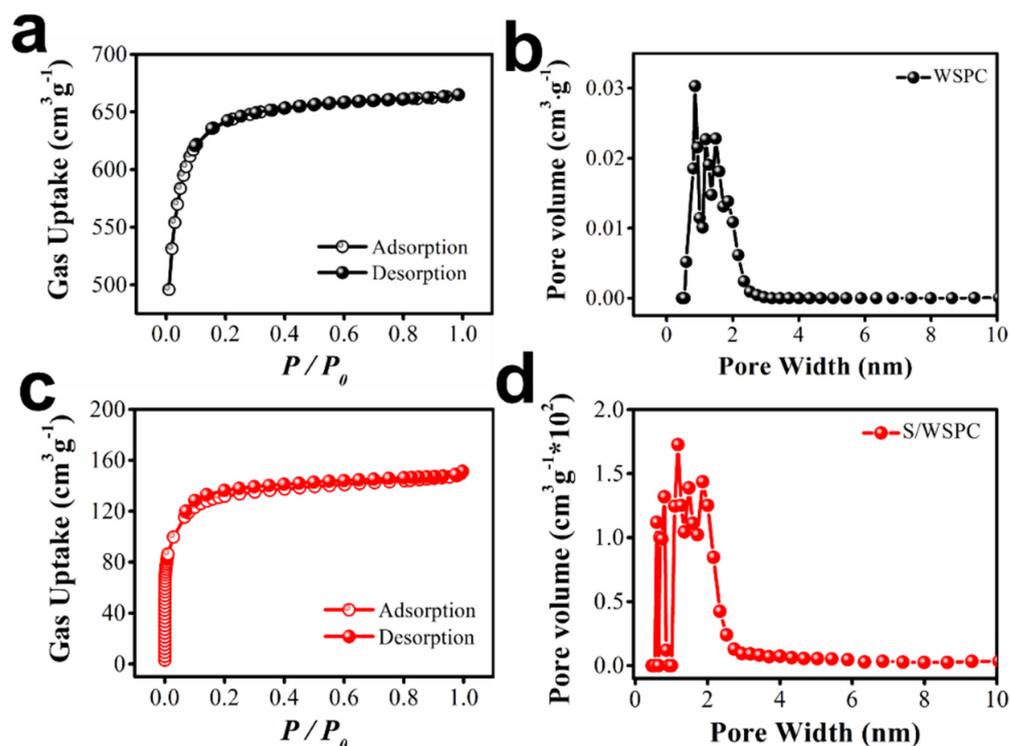

Figure 7. (**a**) N_2 sorption-desorption isotherms and (**b**) pore size distributions of WSPC. (**c**) N_2 sorption-desorption isotherms and (**d**) pore size distributions of S/WSPC.

3.2. Electrochemical Catalytic Performance Test

In the experiment of electrochemical nitrogen reduction to synthesize ammonia, the difference in the current density of the catalyst tested in the saturated electrolyte of Ar and N_2 was the main index to judge whether the catalyst had catalytic nitrogen reduction activity. Before the experiment, high-purity argon with a flow rate of 20 mL/min was first injected for 30 min to exclude the air in the electrolytic cell, and the LSV curve of the catalyst in the Ar saturated electrolyte was tested. Then, high-purity N_2 with the same flow rate was injected for 30 min to test the LSV curve under mild conditions. The comparison curve is shown in Figure 8a. By comparing two LSV curves obtained under the same test conditions, it can be seen that the current density of the catalyst in the N_2 saturated electrolyte was greater than that in the Ar atmosphere, especially when the absolute value of the current density was below -0.65 V. This was due to the presence of stronger hydrogen evolution reactions below -0.65 V contributing a certain current density. The higher current density indicates that the catalyst has an electrochemical reaction under nitrogen saturation conditions, which fully proves that the electrode material has the catalytic activity of nitrogen reduction. It can be seen from the observation of the LSV curve that the current density in the saturated electrolyte of nitrogen and argon starts to differ from -0.25 V. Therefore, we investigated the constant voltage current density test for 2 h under a series of voltages of -0.25 V, -0.35 V, -0.45 V, -0.55 V, and -0.65 V,

respectively, in the experiment. The results are shown in Figure 8b. The difference in current density was small at low voltage, while the current density increased at −0.65 V, which was consistent with the current density results in LSV. The corresponding UV test curve was drawn in Figure 8c. It can be seen from the figure that the curve measured at −0.45 V has the highest absorbance at 655 nm, the characteristic wavelength of NH_4^+, indicating that the concentration of NH_4^+ in the electrolyte of the electrolysis experiment at this voltage was the highest, so −0.45 V was the ammonia production potential with the best catalytic activity of the catalyst. The histogram of ammonia yield and the Faraday efficiency measured under a series of voltages is shown in Figure 8d. It can be seen that with the decrease in voltage, the Faraday efficiency was reduced because some electrons are used for hydrogen evolution reaction, which also affects the electron transport of synthetic ammonia. However, when the voltage was higher, the active potential of the catalyst could not be reached, so the obtained ammonia yield and Faraday efficiency were lower. The optimal activity potential of the S/WSPC catalyst for nitrogen reduction was −0.45 V.
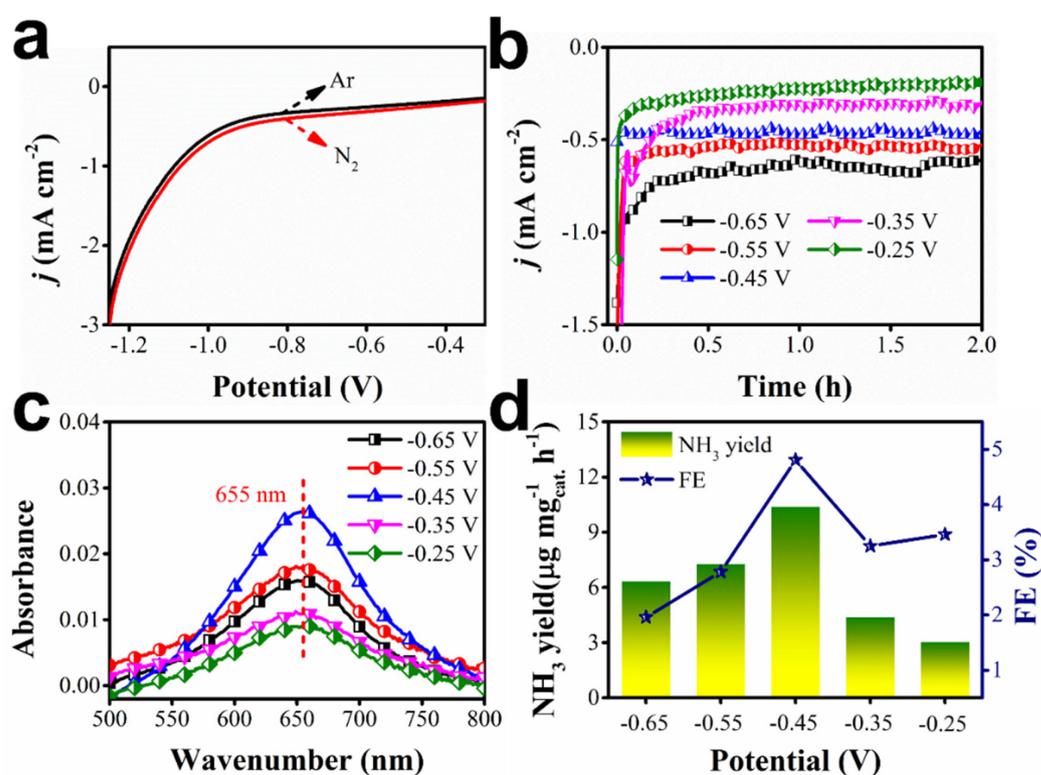

Figure 8. (**a**) LSV curves of S/WSPC in Ar- and N_2-saturated in 0.05 M H_2SO_4, respectively. (**b**) Chronoamperometric curves of S/WSPC at different selected potentials for 2 h. (**c**) UV-vis absorption spectra of the H_2SO_4 electrolyte after electrolysis on the S/WSPC electrode stained with indophenol indicator after charging at various potentials for 2 h under the same conditions. (**d**) NH_3 yields and corresponding FEs of S/WSPC at different selected potentials.

The blank control test was to exclude the influence of other factors in the test on the experimental product. As shown in Figure 9a, the test results of WSPC as a catalyst, pure carbon paper, open circuit voltage, and constant voltage electrolysis experiment in argon saturated electrolyte were, respectively, compared. The test results show that the catalyst has the highest catalytic activity of NH_3 synthesis only when S/WSPC was used as a catalyst and the optimal active voltage was applied in the N_2-saturated electrolyte. The NH_3 measured in WSPC as a catalyst electrolyte may be due to the limited catalytic activity of WSPC itself, resulting in a partial reduction in nitrogen. The trace amount of ammonia obtained from the test of pure carbon paper may come from the N_2 gas or the pollution of the experimental environment. In the open circuit potential, because

there was no electron transmission, the catalytic activity of the catalyst was not activated, so there was basically no NH_3 production, which also proves the necessity of applying potential. The small NH_3 yield measured in the Ar-saturated electrolyte may be due to trace impurities carried in the incoming gas. In order to prove the source of nitrogen in electrocatalytic ammonia synthesis via the catalyst, the experiment conducted continuous alternating cycle consecutive tests of N_2 and Ar for 12 h. The results of NH_3 yield and corresponding Faraday efficiency are shown in Figure 9b. Compared with the argon saturated electrolyte, considerable NH_3 yield was obtained in the N_2 saturated electrolyte, which fully proved that nitrogen was the only nitrogen source in the catalytic ammonia synthesis. The UV absorbance curve of the catalyst in the electrocatalytic N_2 synthesis test repeated for six consecutive times was drawn in Figure 9c, and the corresponding Faraday efficiency was calculated with the amount of charge used in the electrochemical test. As shown in Figure 9d, the NH_3 yield and Faraday efficiency in the six consecutive experiments were basically the same, indicating that the catalyst had good electrochemical stability and structural stability. The catalytic performances of S/WSPC and the reported metal-free NRR catalysts were displayed in Table 2. For catalysts, activity, selectivity, and stability are crucial evaluation indexes, excellent catalysts not only have high catalytic activity but also have unique selectivity for reactants [34]. Therefore, the concentration of by-product N_2H_4 in the electrolyte after the reaction was quantitatively measured using the Watt and Chrisp color development method at the same time. The results showed that no by-product was produced during the reaction, which proved the excellent selectivity of the catalyst for the reduction of the N_2 reaction.
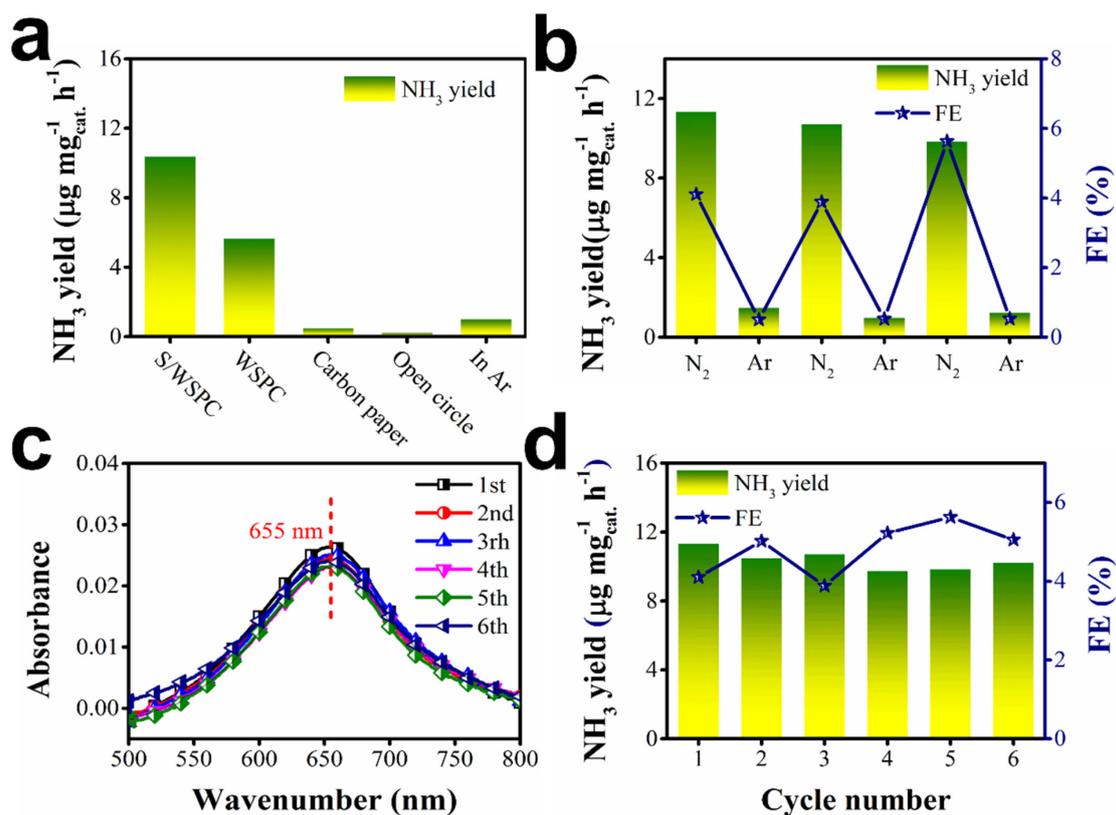

Figure 9. (**a**) NH_3 yields after 2 h electrolysis under different conditions: S/WSPC in N_2, WSPC, Carbon paper, Open circuit, and in Ar at -0.45 V. (**b**)The NH_3 yields and FEs of S/WSPC at the potential of -0.45 V with alternating 2 h cycles between N_2- and Ar-saturated electrolytes. (**c**) UV-vis absorption spectra of the H_2SO_4 electrolyte after electrolysis on the S/WSPC electrode stained with indophenol indicator after charging six cycles for 2 h under the same conditions. (**d**) NH_3 yields and corresponding FEs of S/WSPC during the recycling test 6 times.

Table 2. The catalytic performances of S/WSPC and the reported metal-free NRR catalysts.

Catalyst	Electrolyte	Optimum Potential (V vs. RHE)	NH$_3$ Yield (µg mg^{-1} h^{-1})	Ref.
S/WSPC	0.05 M H$_2$SO$_4$	−0.45	10.39	This work
S-CNS	0.10 M Na$_2$SO$_4$	−0.70	19.07	[25]
BCN	0.10 M HCl	−0.30	7.75	[35]
BNS	0.10 M Na$_2$SO$_4$	−0.80	13.22	[36]
N-doped carbon	0.10 M HCl	−0.20	15.7	[37]

4. Conclusions

In this work, we developed a sulfur-modified walnut shell porous carbon catalyst (S/WSPC) for the electrochemical synthesis of ammonia under mild conditions. The S/WSPC catalyst exhibited a significantly higher ammonia yield (10.39 µg$_{NH3}$ mg$_{cat.}^{-1}$ h^{-1}) than the unmodified walnut shell porous carbon (WSPC) catalyst (5.17 µg$_{NH3}$ mg$_{cat.}^{-1}$ h^{-1}). The porous carbon derived from the walnut shell was used as the main research body, and the biosaccharide-derived microporous carbon with a high specific surface area was obtained. The low-temperature sulfur-modified carbon material was used as the electrocatalytic ammonia synthesis catalyst to systematically study the performance of ammonia synthesis. The electrocatalytic N$_2$ reduction performance of WSPC and S/WSPC was compared and tested, respectively. Combined with the characterization of the physical and chemical structure of the catalyst, it was proved that the presence of sulfur improves the electrocatalytic performance of carbon materials. (1) The presence of pristine sulfur provides the catalyst with hydrophobicity, which helps to inhibit the water-resolved hydrogen competitive reaction and improve the utilization rate of reaction electrons; (2) Sulfur atom doping causes lattice distortion and the polarization effect, which increases the original carbon atom polarizability and creates more defects, and these defects are considered to be effective electrocatalytic active sites for the synthesis of ammonia [37]; (3) The high specific surface area of biomass porous carbon materials provides a rich space for nitrogen adsorption, and the carbon substrate with a high degree of graphitization provides a high-speed channel for rapid electron transport in the electrochemical reaction process, thus promoting the rapid electrochemical reaction. The development of efficient and affordable electrocatalysts is essential for the practical realization of ammonia electrosynthesis. Our work provides a new and promising approach to the development of such catalysts.

Author Contributions: J.W.: Formal analysis, Software, Visualization, Writing—original draft; Z.Z.: Data curation, Investigation; B.L.: Writing—review and editing; Z.W.: Conceptualization, Writing—review and editing; S.W.: Funding acquisition, Resources, Supervision. All authors have read and agreed to the published version of the manuscript.

Data Availability Statement: No new data were created or analyzed in this study. Data sharing is not applicable to this article.

Conflicts of Interest: The authors declare no conflict of interest.

References

1. Martin, A.J.; Tatsuya, S.; Javier, P.-R. Electrocatalytic Reduction of Nitrogen, From Haber-Bosch to Ammonia Artificial Leaf. *Chem* **2019**, *5*, 263–283. [CrossRef]
2. Guo, W.; Zhang, K.; Liang, Z.; Zou, R.; Xu, Q. Electrochemical nitrogen fixation and utilization, theories, advanced catalyst materials and system design. *Chem. Soc. Rev.* **2019**, *48*, 5658–5716. [CrossRef]
3. Suryanto Bryan, H.R.; Du, H.-L.; Wang, D.; Chen, J.; Alexandr, N.S.; Douglas, R.M. Challenges and prospects in the catalysis of electroreduction of nitrogen to ammonia. *Nat. Catal.* **2019**, *2*, 290–296. [CrossRef]
4. Li, L.; Tang, C.; Yao, D.; Zheng, Y.; Qiao, S.-Z. Electrochemical Nitrogen Reduction, Identification and Elimination of Contamination in Electrolyte. *ACS Energy Lett.* **2019**, *4*, 2111–2116. [CrossRef]

5. Yang, X.; Shreya, M.; Thomas, O.; Hou, Y.; Meenesh, S.R.; Joseph, A.G.; Wu, G. Achievements, Challenges, and Perspectives on Nitrogen Electrochemistry for Carbon-Neutral Energy Technologies. *Angew. Chem. Int. Ed.* **2023**, *62*, e202215938. [CrossRef] [PubMed]

6. Muhammad Lbrar, A.; Aya, A.; Brynn, H.D.; Zhao, C. Li-Mediated Electrochemical Nitrogen Fixation, Key Advances and Future Perspectives. *Small* **2023**, 2305616.

7. Chen, G.-F.; Ren, S.; Zhang, L.; Cheng, H.; Luo, Y.; Ding, L.-X.; Wang, H. Advances in Electrocatalytic N_2 Reduction—Strategies to Tackle the Selectivity Challenge. *Small Methods* **2018**, *3*, 1800337. [CrossRef]

8. Chen, X.; Guo, Y.; Du, X.; Zeng, Y.; Gong, C.; Huang, J.; Fan, C.; Wang, X.; Xiong, J. Atomic Structure Modification for Electrochemical Nitrogen Reduction to Ammonia. *Adv. Energy Mater.* **2019**, *10*, 1903172. [CrossRef]

9. Zhang, L.; Chen, G.; Ding, L.-X.; Wang, H. Advanced Non-metallic Catalysts for Electrochemical Nitrogen Reduction under Ambient Conditions. *Chemistry* **2019**, *25*, 12464–12485. [CrossRef]

10. Chen, S.; Siglinda, P.; Claudio, A.; Chalachew, M.; Su, D.; Gabriele, C. Electrocatalytic Synthesis of Ammonia at Room Temperature and Atmospheric Pressure from Water and Nitrogen on a Carbon-Nanotube-Based Electrocatalyst. *Angew. Chem. Int. Ed.* **2017**, *56*, 2699–2703. [CrossRef]

11. Qiu, W.; Xie, X.; Qiu, J.; Fang, W.; Liang, R.; Ren, X.; Ji, X.; Cui, G.; Abdullah, A.M.; Cui, G.; et al. High-performance artificial nitrogen fixation at ambient conditions using a metal-free electrocatalyst. *Nat. Commun.* **2018**, *9*, 3485. [CrossRef] [PubMed]

12. Yin, J.; Zhang, W.; Alhebshi, N.A.; Numan, S.; Alshareef, H.N. Synthesis Strategies of Porous Carbon for Supercapacitor Applications. *Small Methods* **2020**, *4*, 1900853. [CrossRef]

13. Zhang, L.; Lin, J.; Liu, Z.; Zhang, J. Non-noble metal-based catalysts for acetylene semihydrogenation: From thermocatalysis to sustainable catalysis. *Sci. China Chem.* **2023**, *66*, 1963–1974. [CrossRef]

14. Chen, Y.; Zhang, X.; Zhou, Z. Carbon-Based Substrates for Highly Dispersed Nanoparticle and Even Single-Atom Electrocatalysts. *Small Methods* **2019**, *3*, 1900050. [CrossRef]

15. Fu, A.; Wang, C.; Pei, F.; Cui, J.; Fang, X.; Zheng, N. Recent Advances in Hollow Porous Carbon Materials for Lithium-Sulfur Batteries. *Small* **2019**, *15*, e1804786. [CrossRef] [PubMed]

16. Wang, H.; Wang, L.; Wang, Q.; Ye, S.; Sun, W.; Shao, Y.; Jiang, Z.; Qiao, Q.; Zhu, Y.; Song, P.; et al. Ambient Electrosynthesis of Ammonia, Electrode Porosity and Composition Engineering. *Angew. Chem. Int. Ed.* **2018**, *57*, 12360–12364. [CrossRef]

17. Jin, H.; Kim, S.S.; Sandhya, V.; Jeseok, L.; Kwangyeol, L.; Kyoungsuk, J. Electrochemical Nitrogen Fixation for Green Ammonia: Recent Progress and Challenges. *Adv. Sci.* **2023**, *10*, 2300951. [CrossRef]

18. Chen, L.; Huang, Z.; Liang, H.; Gao, H.; Yu, S. Three-Dimensional Heteroatom-Doped Carbon Nanofiber Networks Derived from Bacterial Cellulose for Supercapacitors. *Adv. Funct. Mater.* **2014**, *24*, 5104–5111. [CrossRef]

19. Shehman, A.; Tayyeba, T.; Zaeem, I.M.; Mannan, B.A.; Khush, B.; Umair, S. Recent progress in Pd based electrocatalysts for electrochemical nitrogen reduction to ammonia. *J. Electroanal. Chem.* **2023**, *931*, 117174.

20. Wang, J.; Huang, H.; Wang, P.; Wang, S.; Li, J. N, S synergistic effect in hierarchical porous carbon for enhanced NRR performance. *Carbon* **2021**, *179*, 358–364. [CrossRef]

21. Cong, L.; Yu, Z.; Liu, F.; Huang, W. Electrochemical synthesis of ammonia from N_2 and H_2O using a typical non noble metal carbon based catalyst under ambient conditions. *Catal. Sci. Technol.* **2019**, *9*, 1208–1214. [CrossRef]

22. Ma, X.; Zhao, L.; Song, X.; Zhao, L.; Yu, Z.; Xiao, Z.; Wang, X.; Li, S.; Cao, Y.; Ning, G.; et al. Production of S-doped porous graphene via post-treatment with $MgSO_4$ as sulphur source. *Chem. Eng. J.* **2019**, *359*, 801–809. [CrossRef]

23. Zhao, S.; Wang, J.; Wang, P.; Wang, S.; Li, J. One-step synthesis of N, P co-doped porous carbon electrocatalyst for highly efficient nitrogen fixation. *Nano Res.* **2021**, *15*, 1779–1785. [CrossRef]

24. Liu, X.; Wu, J.; Guo, X. Ternary boron-, phosphorus- and oxygen-doped amorphous nickel nanoalloys for enhanced activity towards the oxygen evolution reaction. *Electrochem. Commun.* **2020**, *111*, 106649. [CrossRef]

25. Xia, L.; Wu, X.; Wang, Y.; Niu, Z.; Liu, Q.; Li, T.; Shi, X.; Asiri, A.M.; Sun, X. S-Doped Carbon Nanospheres, An Efficient Electrocatalyst toward Artificial N_2 Fixation to NH_3. *Small Methods* **2018**, *3*, 1800251. [CrossRef]

26. Shi, Z.; Yang, W.; Gu, Y.; Ting, L.; Sun, Z. Metal-Nitrogen-Doped Carbon Materials as Highly Efficient Catalysts, Progress and Rational Design. *Adv. Sci.* **2020**, *7*, 2001069. [CrossRef]

27. Tian, Y.; Xu, D.; Chu, K.; Wei, Z.; Liu, W. Metal-free N, S co-doped graphene for efficient and durable nitrogen reduction reaction. *J. Mater. Sci.* **2019**, *54*, 9088–9097. [CrossRef]

28. Xia, L.; Yang, J.; Wang, H.; Zhao, R.; Chen, H.; Fang, W.; Asiri, A.M.; Xie, F.; Cui, G.; Sun, X. Sulfur-doped graphene for efficient electrocatalytic N_2-to-NH_3 fixation. *Chem. Commun.* **2019**, *55*, 3371–3374. [CrossRef]

29. Wang, J.; Wang, S.; Li, J. S-Doped three-dimensional graphene (S-3DG), a metal-free electrocatalyst for the electrochemical synthesis of ammonia under ambient conditions. *Dalton Trans.* **2020**, *49*, 2258–2263. [CrossRef]

30. Wang, J.; Wang, S.; Li, J. A metal-free catalyst, sulfur-doped and sulfur nanoparticle-modified CMK-3 as an electrocatalyst for enhanced N_2-fixation. *New J. Chem.* **2020**, *44*, 20935–20939. [CrossRef]

31. Song, P.; Kang, L.; Wang, H.; Guo, R.; Wang, R. Nitrogen (N), Phosphorus (P)-Codoped Porous Carbon as a Metal-Free Electrocatalyst for N_2 Reduction under Ambient Conditions. *ACS Appl. Mater. Interfaces* **2019**, *11*, 12408–12414. [CrossRef] [PubMed]

32. Xiao, S.; Luo, F.; Hu, H.; Yang, Z. Boron and nitrogen dual-doped carbon nanospheres for efficient electrochemical reduction of N_2 to NH_3. *Chem. Commun.* **2020**, *56*, 446–449. [CrossRef] [PubMed]

33. Wang, J.; Kaskel, S. KOH activation of carbon-based materials for energy storage. *J. Mater. Chem.* **2012**, *22*, 23710–23725. [CrossRef]

34. Chen, C.; Yan, D.; Wang, Y.; Zhou, Y.; Zou, Y.; Li, Y.; Wang, S. B-N Pairs Enriched Defective Carbon Nanosheets for Ammonia Synthesis with High Efficiency. *Small* **2019**, *15*, e1805029. [CrossRef]

35. Zhang, X.; Wu, T.; Wang, H.; Zhao, R.; Chen, H.; Wang, T.; Wei, P.; Luo, Y.; Zhang, Y.; Sun, X. Boron Nanosheet: An Elemental Two-Dimensional (2D) Material for Ambient Electrocatalytic N_2-to-NH_3 Fixation in Neutral Media. *ACS Catal.* **2019**, *9*, 4609–4615. [CrossRef]

36. Yang, X.; Li, K.; Cheng, D.; Pang, W.; Lv, J.; Chen, X.; Zang, H.Y.; Wu, X.; Tan, H.; Wang, Y.; et al. Nitrogen-doped porous carbon: Highly efficient trifunctional electrocatalyst for oxygen reversible catalysis and nitrogen reduction reaction. *J. Mater. Chem. A* **2018**, *6*, 7762–7769. [CrossRef]

37. Aykut, C.; Berdan, U.; Ozlem, S.; Hilal, K. Synthesis of in situ N-, S-, and B-doped few-layer graphene by chemical vapor deposition technique and their superior glucose electrooxidation activity. *Int. J. Energy Res.* **2019**, *43*, 8204–8216.